UNIUNEA EUROPEANĂ

GUVERNUL ROMÂNIEI
MINISTERUL MUNCII, FAMILIEI, PROTECȚIEI SOCIALE ȘI PERSOANELOR VÂRSTNICE
AMPOSDRU

Fondul Social European
POS DRU 2007-2013

Instrumente Structurale
2007-2013

MINISTERUL EDUCAȚIEI NAȚIONALE
OIPOSDRU

UNIVERSITATEA „ALEXANDRU IOAN CUZA“ din IAȘI

„ALEXANDRU IOAN CUZA” University of IAŞI

Faculty of Physics

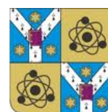

CONTRIBUTIONS REGARDING THE OBTAINING AND CHARACTERIZATION OF FeCuNbSiB AMORPHOUS AND NANOCRYSTALLINE THIN FILMS

Ioana-Laura VELICU

– Summary of the Pd.D. thesis –

SCIENTIFIC COORDINATOR:

Prof. Dr. Maria NEAGU

Iaşi, September, 2013

„ALEXANDRU IOAN CUZA" UNIVERSITY of IAŞI

Faculty of Physics

In attention of:………………………………………………………………………

We bring to your attention that on September 27, at 10:00, in the IV-13 amphitheatre, Mrs. Ioana-Laura VELICU will sustain, in public hearing, the PhD thesis entitled „**Contributions regarding the obtaining and characterization of FeCuNbSiB amorphous and nanocrystalline thin films**" in order to obtain the scientific title of Doctor in Physics.

The doctoral committee has the following members:

Chairman:

Prof. Univ. Dr. Diana Mihaela MARDARE
Director of Doctoral School, Faculty of Physics
„Alexandru Ioan Cuza" University of Iaşi

Scientific coordinator:

Prof. Univ. Dr. Maria NEAGU
Faculty of Physics
„Alexandru Ioan Cuza" University of Iaşi

Referents:

Researcher Dr. Grade I. Horia CHIRIAC
„Alexandru Ioan Cuza" University of Iaşi

Prof. Univ. Dr. Viorel POP
„Babeş-Bolyai" University of Cluj-Napoca

Prof. Univ. Dr. Alexandru SĂLCEANU
„Gheorghe Asachi" Technical University of Iaşi

We invite you with this occasion to attend to the public sustaining of the thesis.

Acknowledgements

My warmest thanks to Mrs. Prof. Dr. Maria Neagu, scientific coordinator of the thesis, for the trust, support and the special training which I received from her during the doctoral program.

I would like to thank to Mr. Prof. Dr. Dumitru Luca for constructing observations and support in conducting the experiments. Also, I would like to thank Mr. Prof. Dr. Gheorghe Popa for very useful discussions and guidance. I am grateful and thank Prof. Dr. Horia Chiriac for real support given to characterize the obtained samples.

I would like to thank my colleagues in the Plasma Physics collective and, especially to Mr. Researcher Dr. Grade III Vasile Tiron for collaboration, friendship and unconditional aid. I would like to thank the Faculty of Physics members, my family, the colleagues and friends that were close to me, encourage and understand me in all this time.

The research was funded from the European Social Fund by the Managing Authority for the Sectoral Operational Programme Human Resources Development 2007-2013 [project POSDRU/CPP 107/DMI 1.5/S/78342] and I would like to thank to the entire project team for financial support.

CONTENTS

Introduction 5
Chapter 1. Soft magnetic materials 6
Chapter 2. Magnetostriction, magnetoimpedance, mechanical properties: theoretical aspects and analysis techniques 7
2.1. Magnetostriction 7
2.2. Magnetoimpedance 7
2.3. Nanoindentation and nanoscratch 8
Chapter 3. Plasma techniques for obtaining thin films 8
Chapter 4. $Fe_{73,5}Cu_1Nb_3Si_{15,5}B_7$ thin films: obtaining and characterization 9
4.1. Techniques and methods 9
4.2. $Fe_{73,5}Cu_1Nb_3Si_{15,5}B_7$ thin films obtained by HiPIMS 10
4.2.1. The influence of experimental parameters on the deposition rate 10
4.2.2. Transport phenomena in plasma magnetron discharge. Influence of experimental parameters on transport phenomena 12
4.2.3. Composition. Structural, topological and magnetic properties 13
4.2.3.1. Amorphous thin films 13
4.2.3.1.1. Composition, structure and topology. Influence of the experimental parameters... 13
4.2.3.1.2. Magnetic behaviour. Coercive magnetic field 15
4.2.3.2. Nanocrystalline thin films 16
4.2.3.2.1. Study of the variation of the magnetization on temperature 16
4.2.3.2.2. Composition, structure, topology 17
4.2.3.2.3. Magnetic behaviour. Coercive magnetic field 19
4.3. $Fe_{73,5}Cu_1Nb_3Si_{15,5}B_7$ thin films obtained by RFMS 20
4.3.1. Influence of the electric power on the deposition rate 20
4.3.2. Composition. Structural, topological and magnetic properties 20
4.3.2.1. Amorphous thin films 20
4.3.2.1.1. Composition, structure and topology. The influence of experimental parameters . 20
4.3.2.1.2. Magnetic behaviour. Coercive magnetic field 20
4.3.2.2. Nanocrystalline thin films 21
4.3.2.2.1. Study of the variation of magnetisation with temperature 21
4.2.3.2.2. Structural characterisation 22
4.2.3.2.2. Magnetic behaviour. Coercive magnetic field 22
4.4. Determination of the saturation magnetostriction of $Fe_{73,5}Cu_1Nb_3Si_{15,5}B_7$ thin films 23
4.5. Determination of the mechanical properties of $Fe_{73,5}Cu_1Nb_3Si_{15,5}B_7$ thin films 24
4.5.1. Modulus of elasticity and hardness 24
4.5.2. Substrate adhesion and the coefficient of friction 25
Chapter 5. $Fe_{73,5}Cu_1Nb_3Si_{15,5}B_7$ thin films: study of the magnetoimpedance effect 26
5.1. Study of the magnetoimpedance effect of mono-layer $Fe_{73,5}Cu_1Nb_3Si_{15,5}B_7$ thin films and $Fe_{73,5}Cu_1Nb_3Si_{15,5}B_7/Cu/Fe_{73,5}Cu_1Nb_3Si_{15,5}B_7$ sandwich 26
5.1.1. Mono-layer $Fe_{73,5}Cu_1Nb_3Si_{15,5}B_7$ 26
5.1.2. Sandwich $Fe_{73,5}Cu_1Nb_3Si_{15,5}B_7/Cu/Fe_{73,5}Cu_1Nb_3Si_{15,5}B_7$ 28
General conclusions 29
References 31

Introduction

In the global context of development of new materials to meet the needs of society, but also the requirements of increasingly demanding industry, the study of magnetic materials is an important direction of contemporary research. With a wide range of properties and possible structures, soft magnetic materials are studied both in solid form as well as powders, ribbons, wires, glass coated wires, thin films etc. [1-6]. The trend of miniaturization of electronics, and more, requires devices and components with complicated forms and reduced dimensions, which is why thin films continue to exhibit considerable amount of interest [7-9].

Due to the remarkable properties (high magnetic permeability and high saturation magnetization, low remanent magnetization and low coercive field, high Curie temperature and good thermal stability of the magnetic properties, low saturation magnetostriction, low magnetic hysteresis loss and low eddy current loss etc.), amorphous and nanocrystalline materials with soft magnetic properties have become viable alternatives in many applications of crystalline magnetic materials, representing an area of current research [10-19].

The FeCuNbSiB alloy system (also known under the trade name FINEMET) is the first and best known Fe-based nanocrystalline alloy system with soft magnetic properties. FeCuNbSiB alloys enjoy a significant amount of attention among researchers due to their high potential for a very wide range of applications: cores for inductive components, electromagnetic waves absorbers, sensitive elements (presence, magnetic field, electric current), actuators, magnetic amplifiers, distribution and signal transformers, active filters etc. [11-13, 16]

The main objectives that we had in mind were:

- ✓ obtaining the amorphous magnetic thin films $Fe_{73,5}Cu_1Nb_3Si_{15,5}B_7$;
- ✓ study of the composition, structural, topological, magnetic, magnetostrictive and mechanical properties and the magnetoimpedance effect of the thin films obtained;
- ✓ study the influence of experimental parameters on some of the properties of thin films / establish optimal experimental parameters to obtain soft magnetic thin films with superior properties;
- ✓ obtaining nanocrystalline thin films of $Fe_{73,5}Cu_1Nb_3Si_{15,5}B_7$.

The techniques used to obtain thin films $Fe_{73,5}Cu_1Nb_3Si_{15,5}B_7$ were:

- **H**igh **P**ower **I**mpulse **M**agnetron **S**puttering – **HiPIMS**;
- **R**adio **F**requency **M**agnetron **S**puttering – **RFMS**.

The induction of nanocrystalline structure was achieved by suitable thermal treatments applied to amorphous precursors.

Chapter 1. Soft magnetic materials

Depending on the value of the coercive magnetic field, magnetic materials can be divided into two classes: soft magnetic materials and hard magnetic materials. For best performance, soft magnetic materials must have a value of the coercive magnetic field as low as possible (of the order of A / m), while the hard magnetic materials must have a value coercive magnetic field as high as possible (> 100 kA / m). There is also a third class of materials called semi-hard materials, with values of coercive magnetic field ranging from 1 kA / m to 100 kA / m [5, 6, 20-22].

Characteristic properties of soft magnetic materials are: high permeability, high saturation magnetization, low residual magnetization, low coercive magnetic field, high Curie temperature and good thermal stability of the magnetic properties, low saturation magnetostriction, low magnetic anisotropy, low magnetic hysteresis loss, low eddy current loss, mechanical resistance to corrosion, ductility and reliability, high electrical resistivity [20-22].

The main classes of soft magnetic alloys are: Fe-Si alloys, Fe-Ni alloys, Fe-Co alloys, soft magnetic ferrites, amorphous alloys and nanocrystalline alloys.

The most popular Fe-based nanocrystalline metallic alloy systems, with soft magnetic properties are: [10, 23, 24]

✓ **$Fe_{73,5}Cu_1M_3(Si_xB_{1-x})_{22,5}$ at% (M = Nb, Mo, Yr, Ta, W etc.)** – known under the trade name **FINEMET**. In nanocrystalline state, this system shows a net superior soft magnetic behaviour compared to the amorphous state, characterized by a unique combination of properties [25-27]: high initial permeability (> 100.000 at 1 kHz); low values of coercive magnetic field (~ 0,5 A/m); low hysteresis losses (core losses P_{Fe} = 38 W/kg at 100 kHz and 0,2 T, lower than the soft magnetic amorphous alloys based on Co); high saturation magnetic induction (~ 1,2 T); low saturation magnetostriction (~ $1 \cdot 10^{-6}$).

✓ **$Fe_{83-86}M_{5-7}B_{2-6}Cu_1$ at% (M = Zr, Nb etc.)** – known under the trade name **NANOPERM**. Higher concentration of the transition metal assures that, in the nanocrystalline state, the soft magnetic properties of this alloy system to be superior to the properties of FeCuNbSiB alloys, leading to increase the saturation magnetic induction up to 1.7 T, and respectively to decrease the saturation magnetostriction [16].

✓ **$(Fe_{1-x}Co_x)_{88}M_7B_4Cu_1$ at% (M = Nb, Hf, Zr etc.)** – known under the trade name **HITPERM**. In nanocrystalline state, HITPERM alloys exhibit soft magnetic properties particularly attractive: high saturation magnetic induction (~ 1,6-2 T) at working temperatures in the range 500-600°C, high Curie temperature, good thermal stability of the magnetic properties (5000 h at 600°C), maximum magnetic permeability of approximately 1800 and core losses of less than 480 W/kg (at 5 kHz and 500°C) [16, 28].

Chapter 2. Magnetostriction, magnetoimpedance, mechanical properties: theoretical aspects and analysis techniques

2.1. Magnetostriction

Magnetostriction is the phenomenon of change in the shape and dimensions of a ferromagnetic material when it is subjected to the action of an external magnetic field. This phenomenon is caused by the change of the magnetization vectors orientation of the magnetic domains, which leads to elongation or contraction of the material in the direction of the external magnetic field [4-6, 20-22]. Positive magnetostrictive materials will elongate in the same direction as the applied external magnetic field, while the negative magnetostrictive materials will shrink in the field direction and will elongate in a direction perpendicular to it. During these deformations, the volume of the magnetized sample remains constant [4]. The effect is reversible, in the absence of the magnetic field the material returning to its original size [5]. If the value of the applied external magnetic field produces the magnetic saturation of the material, the magnetostriction reaches a threshold value, known as saturation magnetostriction, λ_s (material constant) [30]. In the case of thin films, one of the methods for the determination of λ_s is the cantilever method [29-34].

2.2. Magnetoimpedance

The effect of magneto-impedance (MI), is the significant variation in both components (real and imaginary) of the electrical impedance of a magnetic conductor which carry an alternating current (with low amplitude) that is subjected to the action of a static external magnetic field, H_{dc}. Sometimes this change is very high (even up to 700%), in which case the effect is called giant magnetoimpedance effect (GMI). The alternating current, $I = I_0e^{j\omega t}$, of amplitude I_0 and angular frequency $\omega = 2\pi f$ which crosses the wire, generates a transverse magnetic field, H_{ac}, which give rise to magnetization processes in the conductor`s volume. The MI effect is governed by the ability of the body magnetization to respond to the magnetic field generated by the alternating current, depending on its transversal permeability. Therefore, in order to obtain a significant change in electrical impedance of an object, it is ideal to have a magnetic anisotropy in a direction parallel to the magnetic field generated by the alternating current [35-37].

The MI effect was observed in materials in form of wires, glass-covered wires, ribbons and mono-and multilayer thin films [38-45]. This effect can be controlled not only by the frequency and intensity alternating electric current, but also by the direction and intensity of the applied external magnetic field. The MI effect can be measured in three configurations: longitudinal (H_{dc} field direction parallel to the length of the sample), transversal (H_{dc} field direction is perpendicular to the length of the sample) and perpendicular (H_{dc} field direction is perpendicular to the plane of the sample).

2.3. Nanoindentation and nanoscratch

Nanoindentation is a technique that allows the study of mechanical properties of materials at reduced scale. It involves a sequential pressing and withdrawal of a tip (indenter) with known geometry, on a material with plane surface. The data regarding the pressing force and the displacement inside the material contain information which can be used to determine the hardness and the modulus of elasticity. The principle of the method consists in recording the force-displacement curves for a full cycle charge-discharge. Discharge curve is fundamental in determining the mechanical properties of the investigated materials [46-50]. The processing of the data obtained from nanoindentation tests applied to bulk materials or thin films/substrate systems, for which the thin films have the same mechanical properties as the substrates, can be achieved by using Oliver-Pharr model. This model has been developed on the assumption that during the loading phase, the stress may contain irreversible inelastic or plastic deformations, while at unloading, the characteristic curve is purely elastic [50]. If the thin films have different mechanical properties of the substrates that were deposited on, the Oliver Pharr model must be completed with one of the relationships that take into account not only the properties of the analyzed material and the indenter, but also those of the substrates [51, 52].

Adhesion of the thin films on the deposition supports, as well as the coefficient of friction may be examined with the nanoscratch tests [49].

Chapter 3. Plasma techniques for obtaining thin films

Plasma techniques are part of the physical methods of vapour phase deposition and play an increasingly important role in obtaining thin films [53]. In contrast to other techniques for obtaining thin films, plasma techniques and in particular cathodic pulverization, offers a wide range of advantages: simplicity of the physical process involved, ease of pulverising high melting point materials, maintaining stoichiometry in the case of composite targets, good adhesion of the thin film to substrate, the possibility of cooling/avoid the heating of targets during the deposition process, growth and controlled doping of the thin films, obtaining amorphous thin films [53-56].

In its simplest version, cathodic pulverization takes place in the form of a luminescent discharge in an inert gas (mostly Argon) that is at low pressure, in a diode type system, in direct current, between a negatively biased electrode (known as the cathode) and another electrode (anode) or the walls of the enclosure. The cathode should be made of the material to be deposited as thin films, in which case it is also known as the target [53, 57].

The conventional sputtering process is extremely inefficient and, therefore solutions were searched to optimise this process. One of the configurations mostly used for this purpose is the magnetron configuration [58].

Magnetron cathodic pulverization was extended and perfected, working in different modes: DCMS (Direct Current Magnetron sputtering), RFMS (Radio Frequency Magnetron Sputtering), HiPIMS (High Power Impulse Magnetron Sputtering) etc.

Chapter 4. $Fe_{73,5}Cu_1Nb_3Si_{15,5}B_7$ thin films: obtaining and characterization

4.1. Techniques and methods

✓ Amorphous $Fe_{73,5}Cu_1Nb_3Si_{15,5}B_7$ thin films with soft magnetic properties were obtained, using as deposition techniques:

- **H**igh **P**ower **I**mpulse **M**agnetron **S**puttering – **HiPIMS**;
- **R**adio **F**requency **M**agnetron **S**puttering – **RFMS**.

For both deposition techniques, magnetic ribbons with $Fe_{73,5}Cu_1Nb_3Si_{15,5}B_7$ composition have been used (Vacuumschmelze GmbH & Co. KG). The thin films were deposited on glass and silicon substrates.

✓ ***Thickness*** and hence the ***deposition rates*** of the thin films obtained were determined using the *interferometric method*.

✓ ***Thermal treatments*** required to obtain the nanocrystalline structure were conducted in the thermal treatment furnace, in vacuum (10^{-6} Torr).

✓ ***The surface chemical composition*** was analyzed by X-ray photoelectron spectroscopy (XPS) using a PHI 5000 spectrometer VersaProbe (Φ ULVAC-PHI, Inc.).

✓ ***The microstructure*** was analyzed by X-ray diffraction method (XRD), respectively, scanning electron microscopy method (SEM) using a Shimadzu LabX XRD-6000 diffractometer (Bragg-Bretano configuration (θ-2θ) with Kα radiation) respectively, a Jeol JAX-840A microscope (accelerating voltage - 20 kV, magnification - 30.000X, the distance between sample and gun - 10 mm). Phase volume fraction of α-Fe(Si), b.c.c., v_{cr}, the average grain size of α-Fe(Si), b.c.c., D, the inter-planar distance, d, and the lattice parameter, a, were estimated from the diffraction peaks present in the recorded diffractograms [59]. The Si percentage of the nanocrystalline phase Fe(Si) was calculated using the quantitative dependence of the lattice parameter and the percentage of Si of Fe-Si alloys, determined by Bozorth [60].

- ✓ ***Surface topology*** was analyzed by atomic force microscopy (AFM) using a scanning microscope NT-MDT Solver Pro-M, in tapping mode.
- ✓ ***Volume and surface magnetic behaviour*** were analyzed by the flowmetry method, respectively, by magneto-optical Kerr effect [61].
- ✓ ***The crystallization kinetics*** was studied by recording the variation of the magnetization on temperature using a Lakeshore 7410 and magnetic field of 1000 Gauss, as well as by differential scanning calorimetry (DSC) using a Perkin-Elmer 8000 system and a heating rate of 40 °C/min. The characteristic temperatures can be determined either as the abscissa of the intersection point of two tangents to the thermomagnetic curve [62], either by the differential method of Tauxe which tracks the point of maximum curvature of the thermomagnetic curve [63]. The maximum of the second derivative of the thermomagnetic curve occurs at the point of its maximum curvature, and may be a reasonable approximation of some of the characteristic temperatures.
- ✓ ***The mechanical properties*** (Young's modulus, E and hardness, H), ***adhesion*** of the thin films to the deposition substrates, as well as the coefficient of friction of thin films were investigated and determined by nanoindentation and nanoscratch tests, using: *Hysitron TriboLab® nanomechanical Test Instrument* (1 μN - 30,000 μN) and *Nano Indentation Tester* (NHT^2) – CSM Instruments (1.000 μN – 500.000 μN) equipped with a Micro-Scratch Tester (MST) – CSM Instruments. The indenter used was a Berkovich type indenter (in the form of a pyramid with three sides) with diamond tip and radius of curvature of 100 nm. Oliver-Pharr method for calculation was corrected with the linear formula.
- ✓ ***Saturation magnetostriction*** was measured by the cantilever method.
- ✓ During thin films deposition, ***high power impulse magnetron discharge diagnosis*** was achieved by:
  - *Optical and spectral methods* - *laser resonant absorption* measurements (TD-LAS) and *laser induced fluorescence* (TD-LIF); *emission spectroscopy*; *ultra-fast photography*.
  - *Electrical methods* (recording the *temporal evolution of the current intensity on discharge*, respectively, the *voltage*).

4.2. $Fe_{73,5}Cu_1Nb_3Si_{15,5}B_7$ thin films obtained by HiPIMS

4.2.1. The influence of experimental parameters on the deposition rate

The research activities have focused on the study of influence of the experimental parameters (*deposition time*, t, *working gas pressure*, p, *average power*, P_{med}, *voltage pulse duration*, τ, *voltage applied to the target*, U) on the properties of the thin films. Thus, thin films were obtained for: $t = 30 \div 180$ minutes, $p = 8 \div 60$ mTorr, $P_{med} = 30$

÷ 90 W, τ = 4 ÷ 20 µs, U = -0,5 ÷ -1 kV; substrate was either grounded or left floating or negatively polarized.

Optimal deposition conditions were established that allow obtaining thin films with uniform surfaces and superior soft magnetic properties: p = 10 mTorr, P_{med} = 30 W, τ = 4 µs, U = -1 kV, grounded substrate.

The deposition rate of thin films can be controlled by specific parameters of the high power impulse magnetron discharge, such as:

✓ *Working gas pressure.* The deposition rate of thin films grows from 3,2 nm/min to 3,8 nm/min in the range 8-10 mTorr and drops from 3,8 nm/min to 1,4 nm/min in the range 10-60 mTorr (working conditions: P_{med} = 30 W, τ = 4 µs, U = -1 kV). The decrease of the deposition rate with the increase of the working gas pressure is due to the strong thermalisation of the flow of particles from the sputtering process, as long as the initiation of the *self-sputtering regime*.

✓ *Voltage pulse duration and average power.* For the same duration of the voltage pulse, the deposition rate increases approximately 3 times when the average power is increased from 30 W to 90 W, while at the same average power, the deposition rate decreases when the voltage pulse duration increases from 4 µs to 20 µs (Figure 4.1, working conditions: p = 10 mTorr, U = -1 kV).

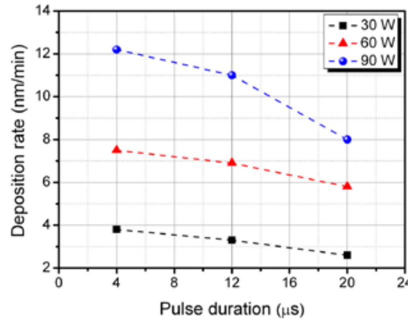

Figure 4.1: Deposition rate dependence on average power and voltage pulse duration.

In order to maintain a constant average power value, the frequency of repetition of the voltage pulses is reduced by approximately an order of magnitude with increasing pulse duration (Table 4.1).

Table 4.1. The values of frequency for different values of the voltage pulse, respectively, the average power.

P (W)	**ν** (Hz)	**τ** (µs)	**P** (W)	**ν** (Hz)	**τ** (µs)	**P** (W)	**ν** (Hz)	**τ** (µs)
30	575	4	60	1250	4	90	1900	4
	107	12		280	12		820	12
	51	20		170	20		500	20

✓ *The voltage applied to the target.* When the voltage applied to the target decreases in absolute value from -1 kV to -0.5 kV, the thin films deposition rate increases linearly from 3.8 nm/min to 6.2 nm/min (working conditions: p = 10 mTorr, P_{med} = 30 W, τ = 4 μs, U = -1 kV).

4.2.2. Transport phenomena in plasma magnetron discharge. Influence of experimental parameters on transport phenomena

We studied the influence of working gas pressure (8-40 mTorr), voltage pulse duration (4-20 μs) and average power (30-90 W) on the phenomena occurring in the vicinity of the target and the substrate, as well as those of transport from the plasma volume utilised for deposition of $Fe_{73,5}Cu_1Nb_3Si_{15,5}B_7$ thin films by HiPIMS technique.

✓ *Working gas pressure.* In Figure 4.2 is presented the dependence of average density of neutral iron $3d^7(^4F)4s$ (calculated on the basis of the measurement TD-LAS) and the aria of the LIF signal, on the pressure of working gas (working conditions: P_{med} = 30 W, τ = 4 μs, U = -1 kV).

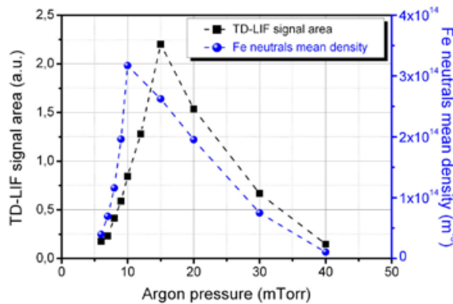

Figure 4.2: Dependence of the average density of neutral iron from the $3d^7(^4F)4s$ level and the aria of the LIF signal on the working gas pressure.

As can be seen, in the vicinity of the substrate, the average density of iron atoms has a maximum value for a working gas pressure of approximately 10 to 15 mTorr. As a result, the pressure of argon whose values fall in this range provides *optimal transport of particles between the target and the substrate*.

The initiation of self-sputtering regime and the compositional changes of the plasma in front of the cathode with increasing pulse duration can be highlighted using ultra-fast photography. In Figure 4.3 are presented recorded images using the ICCD camera for two different durations of the voltage pulse (4 μs and 20 μs) utilising two selective optic filters: a red one with a transmission band in the 695-1100 nm range for optical emission of argon species and a blue one with a transmission band in the 350-400 nm range for optical emission of iron species (working conditions: p = 10 mTorr, P_{med} = 30 W, U = -1 kV). The images clearly show that for short durations of the

voltage pulse (4 µs) optical radiation is dominated by emission from excited argon atoms, while for high voltage pulse duration (20 µs), due to *self-sputtering regime* the optical radiation is dominated by emission from the excited Fe atoms.

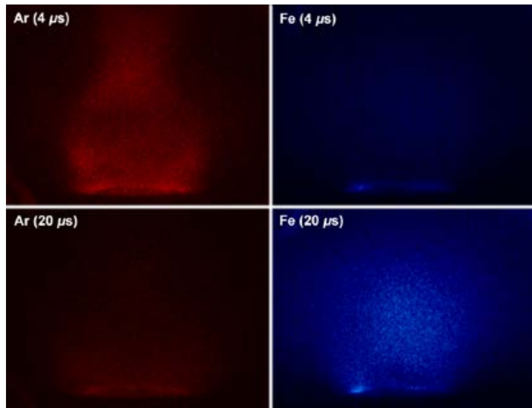

Figure 4.3: ICCD images recorded for voltage pulse durations of 4 µs, respectively 20 µs utilising a red selective optical filter (Ar) and a blue one (Fe).

4.2.3. Composition. Structural, topological and magnetic properties

4.2.3.1. Amorphous thin films

4.2.3.1.1. Composition, structure and topology. Influence of the experimental parameters

✓ *Analysis of the chemical composition of the surface*. The results of the XPS analysis indicated that the thin films surface contains all of the five elements present in the composition of the ribbons used as sputtering targets (Fe, Cu, Nb, Si, B), in atomic percentages approximately equal to those of the ribbons ($Fe_{73,5}Cu_1Nb_3Si_{15,5}B_7$).

✓ *Structural analysis*. The results of XRD and SEM analysis showed that all the thin films obtained by the HiPIMS technique are amorphous, continuous and have compact surfaces.

✓ *Analysis of surface topography*. The results of the AFM analysis showed that the surface topography of the thin films obtained is influenced by certain experimental parameters, such as:

- *Working gas pressure*. The average surface roughness of the thin films increases from 2.6 nm to 4.2 nm in the range of 8-10 mTorr and then decreases to approximately 6 times in the range of 10-60 mTorr (Figure 4.4) (deposition conditions: P_{med} = 30 W, τ = 4 µs, U = -1 kV). Films deposited at low pressures of the working gas (8 mTorr) and also at high pressures (60 mTorr) exhibit non-uniform surfaces (Figure 4.5).

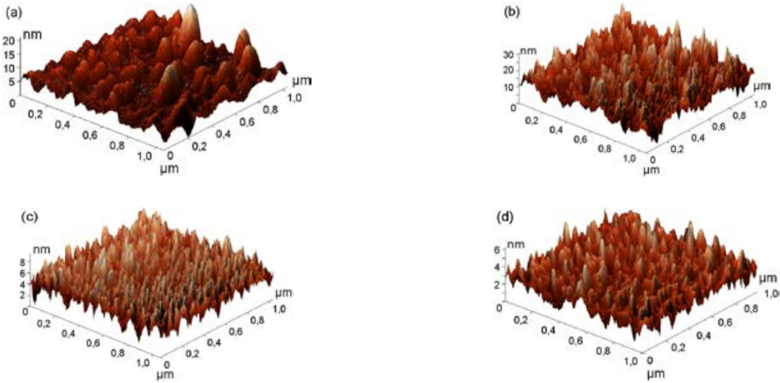

Figure 4.4: AFM 3D images for $Fe_{73,5}Cu_1Nb_3Si_{15,5}B_7$ thin films deposited at: (a) 8 mTorr; (b) 10 mTorr; (c) 40 mTorr; (d) 60 mTorr.

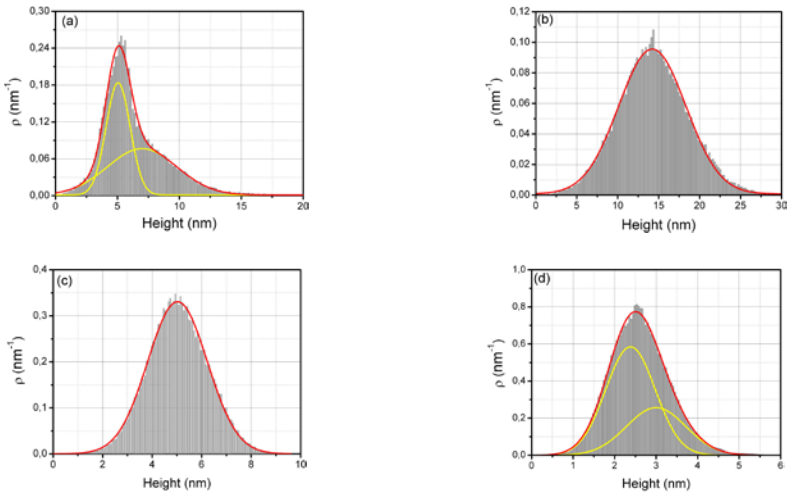

Figure 4.5: Histograms of the heights of surface peaks for $Fe_{73,5}Cu_1Nb_3Si_{15,5}B_7$ thin films deposited at: (a) 8 mTorr; (b) 10 mTorr; (c) 40 mTorr; (d) 60 mTorr.

- *The voltage applied to the target*. The decrease in absolute value of voltage applied to the target from -1 kV to -0,5 kV leads to films with non-uniform surfaces and average roughness of approximately 1,6 times higher.
- *Substrate polarisation*. The polarization of the substrate allows obtaining of thin films with average surface roughness smaller with approximately 57%, but with non-uniform surfaces.

4.2.3.1.2. Magnetic behaviour. Coercive magnetic field

✓ *The influence of the thickness and pressure of the working gas*. For thin films obtained at P_{med} = 30 W, τ = 4 μs, U = -1 kV, in Figure 4.6 (a and b) is presented the dependence of the volume and the surface coercive magnetic fields , H_{cv} şi H_{cs}, on:

- thin films thickness for two samples deposited at different pressures of the working gas: 10 mTorr, respectively 60 mTorr (Figure 4.6a);
- working gas pressure (Figure 4.6b).

Thin films of different thicknesses were obtained by varying the deposition time from 30 minutes to 180 minutes.

Analysing the presented results, it can be shown that:

- for the same deposition time, the thickness of thin films decreases to approximately 2.7 times with the increase of argon pressure from 10 mTorr to 60 mTorr;
- for the same thickness, thin films deposited at different pressures of working gas have different coercive magnetic fields;
- the values of volume and surface coercive magnetic fields are approximately equal;
- the values of H_{cv} şi H_{cs} decrease with the increase of the thin films thickness. For the samples deposited at 10 mTorr pressure, the decrease is approximately 85% (H_{cv}) and 80% (H_{cs}) for a thickness increase from 110 nm to 700 nm. For samples deposited at 60 mTorr pressure, the decrease is approximately 75% (H_{cv}) and 73% (H_{cs}) for a thickness increase from 40 nm to 260 nm.

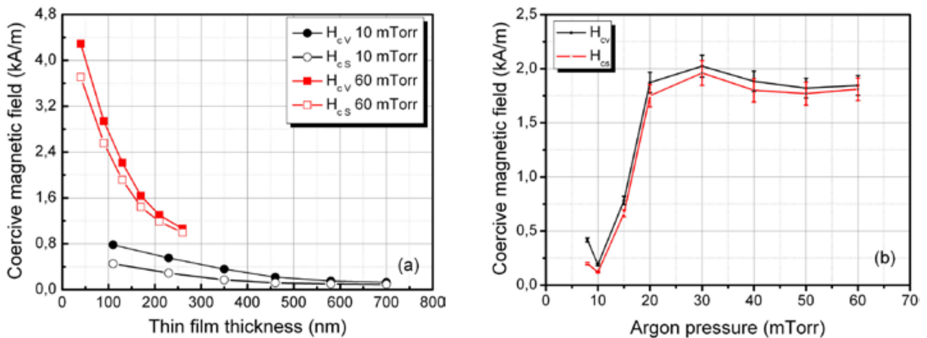

Figure 4.6: Dependence of the volume and surface coercive magnetic field on: (a) thin films thickness; (b) working gas pressure.

In order to describe mathematically the dependence of H_{cv} on the thin films thickness, the curves presented in Figure 4.6a were fitted using the program Origin, with the function $\mathbf{H_c = C/t^n}$ (*t* – thin film thickness, *C* and *n* – constants whose values

depend on the state of the thin films and the equipment and conditions used to produce them). The obtained values for constants C and n are: 39133 and 0,84 (p = 10 mTorr); 48286 and 0,67 (p = 60 mTorr). The difference between the decrease rates of the volume coercive magnetic field for thin films deposited at different working gas pressures may be due to topography, as well as to different mechanical tensions induced during the deposition process.

✓ *The influence of average power and the voltage pulse duration*. The volume coercive magnetic field decreases by approximately 20% when the average power increases from 30 W to 90 W (working conditions: p = 10 mTorr, τ = 4 µs, U = -1 kV) and increases with approximately 20% when the voltage pulse duration increases from 4 µs to 10 µs (working conditions: p = 10 mTorr, P_{med} = 30 W, U = -1 kV).

✓ *The influence of applied voltage on the target*. The volume coercive magnetic field decreases with approximately 40% when the absolute value of the voltage applied on the target decreases from -1 kV to -0,5 kV.

4.2.3.2. Nanocrystalline thin films

In order to obtain nanocrystalline state, and thus, to improve soft magnetic properties, amorphous thin films were treated isotherm, for one hour, in a thermal treatment furnace, at suitable temperatures, set both by thermomagnetic analysis (the study of variation of magnetization with temperature) and by differential scanning calorimetry analysis.

4.2.3.2.1. Study of the variation of the magnetization on temperature

In Figure 4.7 are presented for comparison thermomagnetic curves normalised to unity : ribbon utilised as target, thin film deposited at 10 mTorr pressure (460 nm thickness, silicon support, deposition conditions: P_{med} = 30 W, τ = 4 µs, U = -1 kV) and thin film deposited at 20 mTorr pressure (700 nm thickness, silicon support, deposition conditions: P_{med} = 30 W, τ = 4 µs, U = -1 kV), as well as the DSC curve which correspond to the thin film deposited at p = 20 mTorr pressure. Also in this figure are represented the lengths L_i, defined as the vertical distance between the point whose abscissa is the Curie temperature of ferromagnetic amorphous phase and the horizontal line L_o. The size of L_i is directly proportional to the amount of the residual amorphous phase. In Figure 4.8 is presented the determination of the Curie temperature of the amorphous ferromagnetic phase using Tauxe`s differential method, for the three cases mentioned above.

The values of the Curie temperature of the ferromagnetic amorphous phase, T_c^{am}, the first crystallization temperature, T_x, and the Curie temperature of the ferromagnetic nanocrystalline phase α-Fe(Si), T_c^{cr}, for the ribbon and the two thin films deposited at different pressures of the working gas, are presented in Table 4.2.

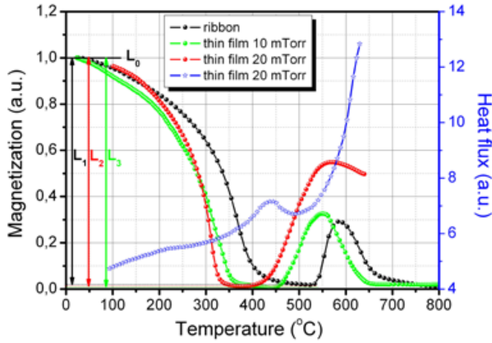

Figure 4.7. Thermomagnetic curves normalized to unity for ribbon and thin films deposited at different pressure of working gas.

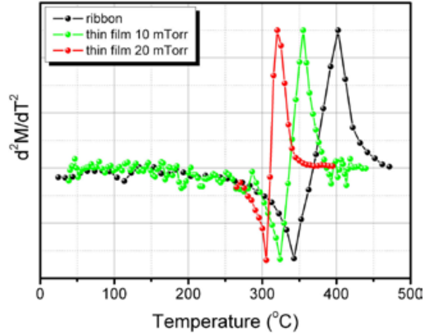

Figure 4.8. Determination of the Curie temperature of ferromagnetic amorphous phase using Tauxe`s differential method for ribbon and thin films deposited at different argon pressures.

Table 4.2. Characteristic temperatures for ribbon and thin films obtained in different conditions

	T_c^{am} (°C)	T_x (°C)	T_c^{cr} (°C)
ribbon	402	530	680
Sample 1 (10 mTorr)	355	460	640
Sample 2 (20 mTorr)	320	440	–

In the case of the two thin films, all three characteristic temperatures have smaller values compared to that of the ribbon. The temperature differences between the ribbon and the two thin films are in accordance with the data from literature for FeCuNbSiB alloys [64].

4.2.3.2.2. Composition, structure, topology

✓ XPS analysis indicated that after the thermal treatment, the surface chemical composition of $Fe_{73,5}Cu_1Nb_3Si_{15,5}B_7$ thin films does not change.

✓ Taking into account the results of the thermomagnetic analysis, the obtained samples were isothermally treated for an hour in vacuum, in the thermal treatment furnace at temperatures in the range 400-525°C. Figure 4.9 presents diffractograms for $Fe_{73,5}Cu_1Nb_3Si_{15,5}B_7$ thin films with 460 nm thickness (deposition conditions: p = 10 mTorr, P_{med} = 30 W, τ = 4 μs, U = -1 kV) recorded before and after thermal treatments at high temperatures. After the thermal treatment conducted at 400 °C, the alloy is still predominantly amorphous, the result being in accordance with the information provided by thermomagnetic analysis. The thermal treatment at 450 °C initiates the crystallisation process, resulting in the occurrence of α-Fe(Si) b.c.c. grains, immersed in a residual amorphous matrix Fe-Nb-B. This is indicated by the

presence of diffraction peaks characteristic to this phase, associated with the crystallographic planes (110), (200) and (211). Figure 4.10 presents the SEM image of the surface of the thin film heat-treated at a temperature of 475 °C, image that indicates the existence of a uniform and ultra-fine grain structure (with an average size below 15 nm) embedded in an amorphous matrix. The results are consistent with those obtained by estimating the average size of the nanocrystalline grains based on the results of X-ray diffraction analysis.

Table 4.3 presents quantitative information on:

- structural parameters (volume fraction of α-Fe(Si) b.c.c. phase, v_{cr}, The average grain size of α-Fe(Si) b.c.c., *D*, inter-planar distance, *d*, and the lattice parameter, *a*) estimated from the diffraction peak (110);
- the diffraction angle , *θ*, corresponding to the peak (110);
- the percentage of silicon of nanocrystalline phase α-Fe(Si), *Si (at%)*.

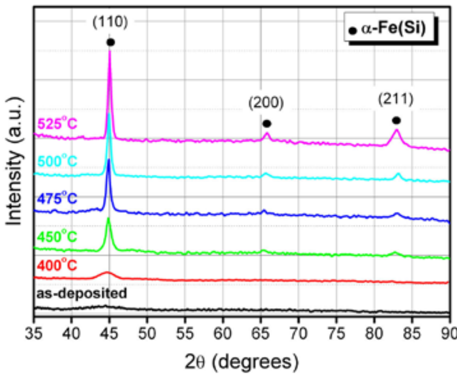

Figure 4.9: $Fe_{73,5}Cu_1Nb_3Si_{15,5}B_7$ thin films diffractograms, recorded before and after the thermal treatments.

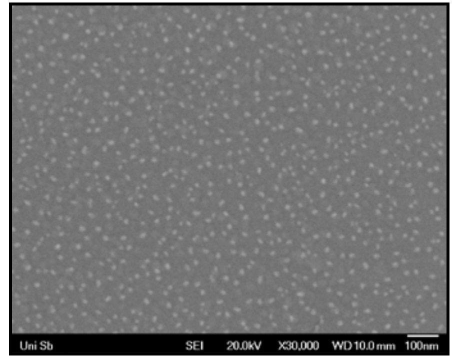

Figure 410: SEM image of a $Fe_{73,5}Cu_1Nb_3Si_{15,5}B_7$ thin film heat treated for 60 minutes at 475 °C.

Table 4.3. Structural parameters, the diffraction angle and the percentage of silicon in the nanocrystalline phase α-Fe(Si) for $Fe_{73,5}Cu_1Nb_3Si_{15,5}B_7$ thin films heat-treated for one hour at the indicated temperatures.

t (°C)	v_{cr} (%)	D (nm)	θ (grade)	d (Å)	a (Å)	Si (at%)
450	45.7	11	22.42	2.019	2.855	6.70
475	53.6	14	22.45	2.016	2.851	10.68
500	61.1	17	22.47	2.014	2.849	11.63
525	65.4	18	22.52	2.011	2.844	14.04

The volume fraction of α-Fe(Si) b.c.c phase increases with the increase of the treatment temperature. This is confirmed by the results presented in Figure 4.8 (the intensity of the diffraction peak (110) increases as the temperature increases, indicating the increase in volume fraction of the crystalline phase). The average grain

size of α-Fe(Si) b.c.c. increases gradually with increasing the treatment temperature. Another thing that is apparent from the data presented in this table is that with the increase of the treatment temperature, the diffraction peaks are slightly shifted to higher angles. This is due to the fact that with the increase in the average size of the nanocrystalline grains, the silica content increases, thereby leading to a decrease in the lattice parameter of the body-centered cubic lattice α-Fe(Si) than that of pure iron (a = 2,866 Å) and thus to the increase of the diffraction angle value.

4.2.3.2.3. Magnetic behaviour. Coercive magnetic field

Figure 4.11 (a and b) presents for a thin film of 460 nm thickness (deposition conditions: p = 10 mTorr, P_{med} = 30 W, τ = 4 μs, U = -1 kV):

- the volume coercive magnetic field dependence on the temperature of the thermal treatment (Figure 4.11a);
- magnetic hysteresis cycles normalised to unity, corresponding to the volume magnetisation for the as-deposited state, as well as after the thermal treatments, performed at 475 °C and 525 °C (Figure 4.11b).

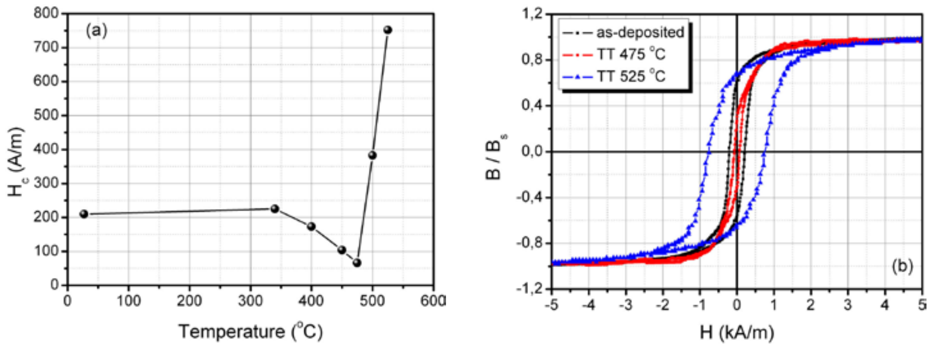

Figure 4.11: (a) The volume coercive magnetic field dependence on the temperature of the thermal treatment; (b) Magnetic hysteresis curves normalised to unity corresponding to volume magnetisation, recorded before and after the thermal treatments performed at 475 °C and 525 °C.

When the thermal treatment temperature increases to the value of 475 °C, the coercive magnetic field decreases by approximately 70%. The minimum coercive magnetic field value (recorded after thermal treatment at 475 °C) corresponds to the situation in which the alloy has ultrafine grain structure α-Fe(Si) b.c.c., with the average size of approximately 14 nm and volume fraction of approximately 53.6%, immersed in an amorphous residual matrix. Further increasing the temperature to the value of 525 °C, H_c presents a rapid growth tendency, up to approximately 750 A/m, indicating the degradation of the soft magnetic properties of the thin films. The decrease in coercive magnetic field with increasing temperature up to a temperature value considerably lower than the first crystallization temperature (T_x ~ 460 °C), is due

to the relaxation processes of induced internal stresses during the deposition process. The decrease in coercive magnetic field in the range between this temperature and the temperature at which it reaches the minimum value, is due to structural changes and, respectively, on the occurrence of α-Fe(Si) b.c.c. nanocrystalline grains.

4.3. $Fe_{73,5}Cu_1Nb_3Si_{15,5}B_7$ thin films obtained by RFMS

4.3.1. Influence of the electric power on the deposition rate

Research has focused on studying the influence of sample thickness and the electric power on the thin films properties. Amorphous thin films were obtained with different thicknesses varying the electric power from 50 W to 70 W, for values of the deposition time from 30 minutes to 120 minutes. The deposition rate of the thin films increases linearly from 1.7 nm/min to 2.6 nm/min when the electric power increases from 50 W to 70 W.

4.3.2. Composition. Structural, topological and magnetic properties

4.3.2.1. Amorphous thin films

4.3.2.1.1. Composition, structure and topology. The influence of experimental parameters

✓ *Analysis of the chemical composition of the surface*. As in the case of the samples obtained by the HiPIMS technique, at the thin films surface it can be found all the five components present in the composition of the ribbons utilised as sputtering target (Fe, Cu, Nb, Si, B), in atomic percentages approximately equal to those of the ribbons.

✓ *Structural analysis*. XRD analysis results showed that all thin films obtained by RFMS technique, are amorphous.

✓ *Analysis of surface topography*. According to the AFM analysis, the thin films obtained by RFMS technique present uniform surfaces, with average roughness values of less than 2% of their thickness.

4.3.2.1.2. Magnetic behaviour. Coercive magnetic field

✓ *The influence of thin film thickness*. In Figure 4.12 is presented the volume and surface coercive magnetic field on the thickness of the thin films. The data presented were obtained for thin films deposited at a power of 60 W, the deposition time varying from 30 minutes to 120 minutes. H_{cv} and H_{cs} decrease by the same law, by approximately 60% when the thickness of the thin films increases from 60 nm to 250 nm. The mathematical description of the volume coercive magnetic field dependence on the thin films thickness was achieved by fitting the curve shown in Figure 4.12 with a function described by the relationship $\mathbf{H_c = C/t^n}$. In this case, the values of constants C and n are 94026 and, respectively, 0,6.

✓ *The influence of electric power*. Coercive magnetic field dependence on the electric power is presented in Figure 4.12. The data presented were obtained for a deposition time of 120 minutes. H_{cv} decreases with 25% (from 4 kA/m to 3 kA/m) when the electric power increases from 50 W to70 W.

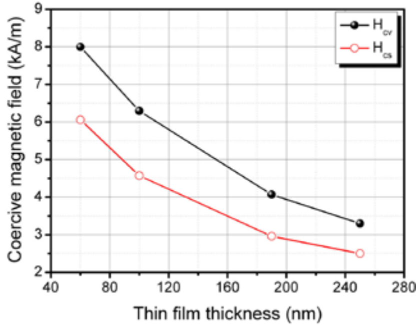

Figure 4.12: H_{cv} and H_{cs} dependence on the thickness of the thin films.

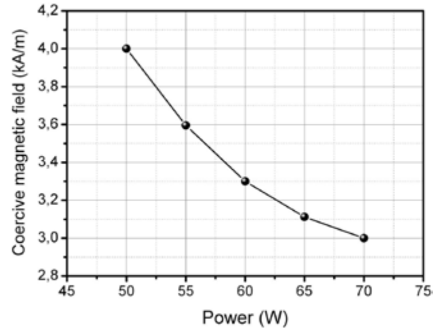

Figure 4.13: The dependence of the volume coercive magnetic field on the electric power.

4.3.2.2. Nanocrystalline thin films

4.3.2.2.1. Study of the variation of magnetisation with temperature

Figure 4.14 presents a thermomagnetic curve normalised to unity, recorded for a thin film with 380 nm thickness, deposited on silicon support (P = 60 W). In Figure 4.15 is presented the determination of the Curie temperature of the ferromagnetic amorphous phase by Tauxe`s differential method. Also in this case, the characteristic temperatures values (the Curie temperature of the ferromagnetic amorphous phase, the first crystallization temperature and the Curie temperature of the ferromagnetic nanocrystalline phase α-Fe(Si)) of the thin films, are smaller than those of the ribbons used as targets.

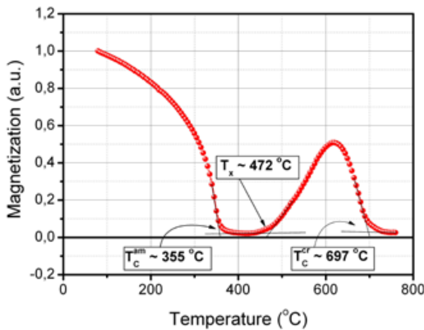

Figure 4.14: Thermomagnetic curve normalised to unity for $Fe_{73,5}Cu_1Nb_3Si_{15,5}B_7$ thin film obtained by RFMS.

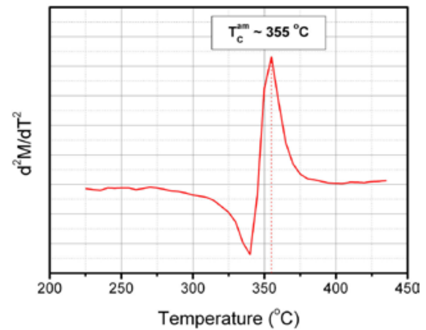

Figure 4.15: Determination of the Curie temperature of the ferromagnetic amorphous phase by Tauxe`s differential method.

4.2.3.2.2. Structural characterisation

In order to induce the nanocrystalline phase, taking into account the information provided by thermomagnetic analysis, the amorphous thin films were heat-treated for 60 minutes at temperatures in the range 200-550 °C.

Figure 4.16 presents recorded diffractograms for $Fe_{73,5}Cu_1Nb_3Si_{15,5}B_7$ thin films, with 250 nm thickness, in the as-deposited state, as well as after they were treated at temperatures in the range 250-550 ^{o}C. After thermal treatments performed at temperatures in the range 250-450 °C, the amorphous structure remains unchanged. After treatment at 500 °C, however, in the recorded diffractograms, a peak centered around the value $2\theta \approx 45^{o}$, appears. Besides this, two other diffraction peaks, with very low intensity, appear. Thus, instead of the amorphous phase, the corresponding diffractogram indicates through the presence of diffraction peaks associated with the crystallographic planes (110), (200) and (211), the existence of a ferromagnetic nanocrystalline phase α-Fe(Si).

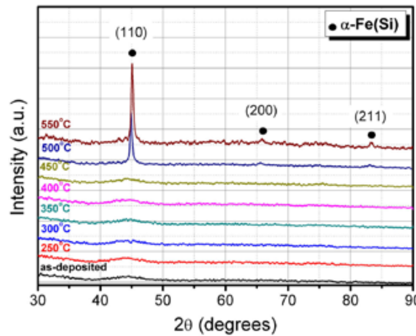

Figure 4.16: Diffractograms for $Fe_{73,5}Cu_1Nb_3Si_{15,5}B_7$ thin films in as-deposited and heat-treated state.

From the diffraction peak (110) were estimated the structural parameters (the crystalline fraction of α-Fe(Si) b.c.c. phase, the average grain size α-Fe(Si) b.c.c., the inter-planar distance and the lattice parameter) specific to the studied alloy and to its current state. For thermal treatment temperatures between 500 ^{o}C and 550 ^{o}C, the volume fraction of α-Fe(Si) b.c.c. phase increases with approximately 24%, and the average grain size α-Fe(Si) b.c.c. increases with approximately 33%. Increasing the thermal treatment temperature, the angles at which diffraction peaks occur are slightly shifted to higher values.

4.2.3.2.2. Magnetic behaviour. Coercive magnetic field

Figure 4.17 presents hysteresis cycles normalised to unity , recorded before and after thermal treatments at 300 ^{o}C, 450 ^{o}C, 500 ^{o}C and 550 ^{o}C, corresponding to volume magnetisation of a thin film with 250 nm thickness, deposited on glass support

(P = 60 W). In Figure 4.18 is presented the dependence of the volume coercive magnetic field on the thermal treatment temperature.

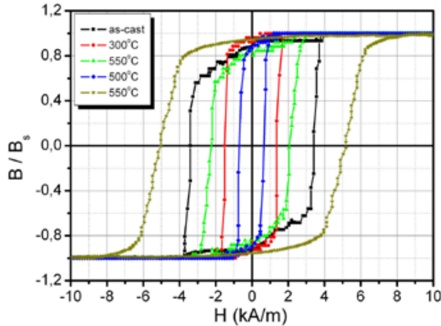

Figure 4.17: Hysteresis curves recorded before and after thermal treatment.

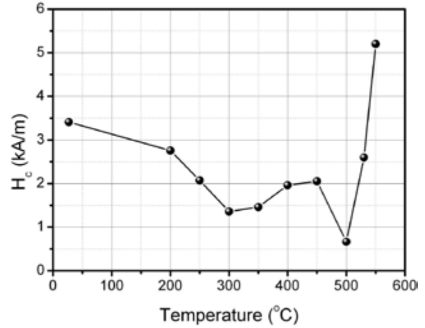

Figure 4.18: Dependence of the coercive magnetic field on the treatment temperature.

After thermal treatment performed on the temperature range 200-500 °C, the value of the magnetic coercive field, presents in general, a tendency to decrease. The decrease to a temperature well below the first crystallization temperature (T_x ~ 472 °C) is due to internal stress relaxation processes. The decrease in volume coercive magnetic field in the interval between this temperature and the temperature at which it reaches the minimum value (500 °C), is due to structural changes, and respectively, on the occurrence of α-Fe(Si) b.c.c. nanocrystalline grains. The minimum value of H_{cv} (664 A/m) is approximately 5 times smaller than that corresponding to as-deposited thin films and corresponds to the situation in which the alloy has ultrafine grain structure α-Fe(Si) b.c.c., with an average size of approximately 15 nm and volume fraction of approximately 53.5%, immersed in a residual amorphous matrix. When the treatment temperature increases from 500 °C to 550 °C, the coercive magnetic field increases by approximately 7,8 times, to the value 5,2 kA/m, indicating the degradation of soft magnetic properties.

4.4. Determination of the saturation magnetostriction of $Fe_{73,5}Cu_1Nb_3Si_{15,5}B_7$ thin films

The saturation magnetostriction of thin films deposited using both techniques was determined by the cantilever method. The values obtained are approximately $23\cdot10^{-6}$ for the amorphous thin films and an order of magnitude lower (~$1\cdot10^{-6}$) for the nanocrystalline thin films.

4.5. Determination of the mechanical properties of $Fe_{73,5}Cu_1Nb_3Si_{15,5}B_7$ thin films

4.5.1. Modulus of elasticity and hardness

Using the procedure of nanoindentation, the hardness, *H*, the reduced modulus of elasticity, E_r, and the effective modulus of elasticity, *E*, of amorphous $Fe_{73,5}Cu_1Nb_3Si_{15,5}B_7$ thin films, deposited on glass supports by HiPIMS technique, as well as RFMS technique, were determined. The mechanical properties of the substrates on which the deposit were made, were also analysed.

Figure 4.19 (a and b) presents a force-displacement curve (Figure 4.19a) and the dependence of the effective and reduced modulus of elasticity and of hardness, on the penetration depth of the indenter (Figure 4.19b), for glass utilised as deposition support. The average value of the effective modulus of elasticity an of hardness is approximately 60 GPa and, respectively, 5,5 GPa (not depending on the penetration depth of the indenter).

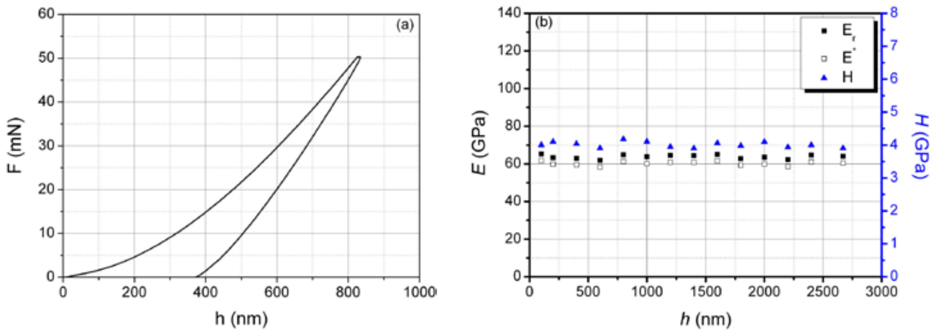

Figure 4.19: (a) Force-displacement curve; (b) Dependence of the effective and reduced modulus of elasticity and of hardness on the penetration depth of the indenter for glass substrate.

Figure 4.20 (a and b) present force-displacement curves (Figure 4.20a) and the dependence of the reduced modulus of elasticity and of hardness on the normalised penetration depth (penetration depth, *h*, normalized to the thickness of the analysed thin film, *t*) (Figure 4.20b) for $Fe_{73,5}Cu_1Nb_3Si_{15,5}B_7$ thin film with 410 nm thickness deposited by HiPIMS technique on glass support (p = 10 mTorr, P_{med} = 30 W, τ = 4 µs, U = -1 kV). As the penetration depth of the indenter increases, both E_r and *H* present a trend of rapid growth to maxim values of approximately 140 GPa and 9 GPa. These values remain constant for a very small displacement of the indenter, between 8% and 15% of the analysed thin film`s thickness. According to the literature, these values are those that describe the most accurate the intrinsic properties of the analysed thin film, without being affected by the existing imperfections on its surface or by the presence of the substrate on which it was deposited [49]. When the glass substrate begins to make its presence felt, the modulus of elasticity and the hardness start decreasing. At first this decrease is very rapid, and when the indenter penetrates into the glass support

(h / t > 1), it becomes more and more slowly, showing a tendency to saturation at values approximately equal to the ones previously determined for the glass substrate.

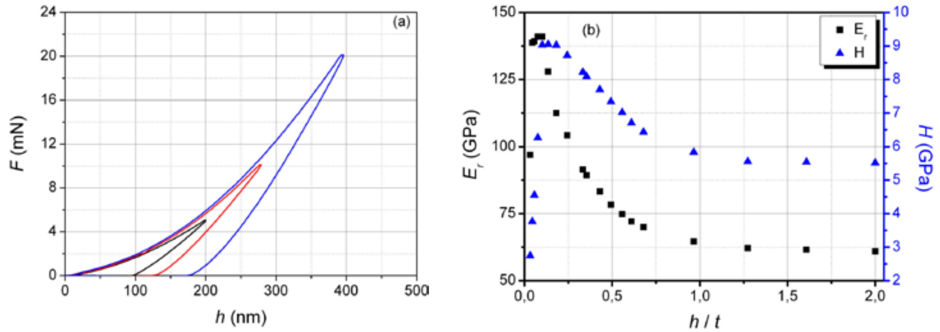

Figure 4.20: (a) Force-displacement curves; (b) Dependence of the reduced modulus and hardness on the normalised penetration depth for a $Fe_{73,5}Cu_1Nb_3Si_{15,5}B_7$ thin film.

The value of the reduced modulus of elasticity of $Fe_{73,5}Cu_1Nb_3Si_{15,5}B_7$ thin films (calculated using the linear formula for the case in which the penetration depth of the indenter is between 8% and 15% of the thickness of the film) is 146 GPa.

4.5.2. Substrate adhesion and the coefficient of friction

Adhesion to deposition substrates, as well as the coefficient of friction of amorphous $Fe_{73,5}Cu_1Nb_3Si_{15,5}B_7$ thin films deposited by HiPIMS technique, as well as by RFMS technique on glass supports, were studied by nanoscratch tests.

During the study of the adhesion of thin films on glass substrates, the force on the indenter was progressively increased from 0,03 N to 12 N, with a rate of 12 N/min. Scratch length was 4 mm.

Figure 4.21 (a, b and c) presents the surface morphology of the thin film, along the scratch, at different times of the nanoscratch test: the first cracks of $Fe_{73,5}Cu_1Nb_3Si_{15,5}B_7$ thin film, occurred at F = 3,48 N, (Figure 4.21a), first delamination occurred at F = 8,16 N (Figure 4.21b) and the complete delamination of the thin film occurred at F = 10,13 N (Figure 4.21c).

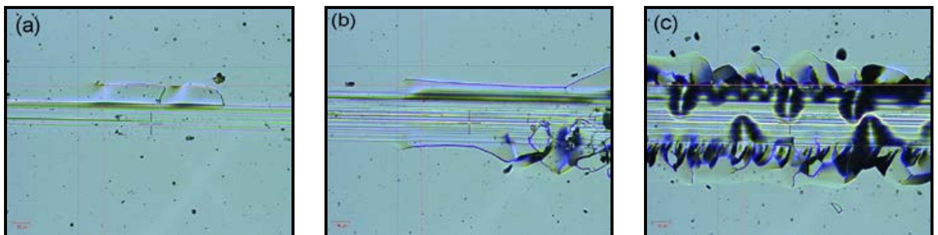

Figure 4.21: The results of the thin films adhesion to glass supports analysis.

The coefficient of friction of the thin films was studied by carving a number of scratches on the sample on a distance of 6 μm, using a force of 1 mN. The results obtained indicated a mean value for the coefficient of friction of about 0.11.

Chapter 5. $Fe_{73,5}Cu_1Nb_3Si_{15,5}B_7$ thin films: study of the magnetoimpedance effect

5.1. Study of the magnetoimpedance effect of mono-layer $Fe_{73,5}Cu_1Nb_3Si_{15,5}B_7$ thin film and $Fe_{73,5}Cu_1Nb_3Si_{15,5}B_7/Cu/Fe_{73,5}Cu_1Nb_3Si_{15,5}B_7$ sandwich

MI effect has been studied in longitudinal configuration (LMI) and transverse (TMI) for mono-layer ($Fe_{73,5}Cu_1Nb_3Si_{15,5}B_7$) thin films, as well as for sandwich systems ($Fe_{73,5}Cu_1Nb_3Si_{15,5}B_7/Cu/Fe_{73,5}Cu_1Nb_3Si_{15,5}B_7$). The data to be presented below belong to mono-layer and sandwich thin films, with the thickness of the $Fe_{73,5}Cu_1Nb_3Si_{15,5}B_7$ thin films of 600 nm, deposited by HiPIMS technique (deposition conditions: p = 10 mTorr, P_{med} = 30 W, τ = 4 μs, U = -1 kV).

5.1.1. Mono-layer $Fe_{73,5}Cu_1Nb_3Si_{15,5}B_7$

Figure 5.1 (a and b) and Figure 5.2 (a and b) present the dependence of the ratio ΔZ/Z (%) (LMI and TMI) on the frequency of the alternating current and the intensity of the applied external magnetic field for a mono-layer thin film, before (Figure 5.1 (a and b)) and after the thermal treatment carried out for an hour at the 475 ^oC temperature (Figure 5.2 (a and b)). The chosen thermal treatment conditions correspond to the situation in which the volume coercive magnetic field has minimum value. For the LMI measurements (Figure 5.1a and Figure 5.2a) are also presented the hysteresis cycles normalised to unity.

As can be seen:

➢ Both before and after the thermal treatment:

- LMI profiles present two peaks of equal intensity, symmetrical with respect to the applied external magnetic field. The value of the magnetic field which corresponds to the maximum of a peak, it`s the value of the anisotropy magnetic field, H_k, which can be determined from the magnetic hysteresis curves (Figure 5.4a and Figure 5.5a) [36]. After the thermal treatment, the value of H_k decreases with approximately 40%, because of tension relaxations, as well as the structural changes inside the material`s volume.

- TMI profiles show a single peak, centered around 0 Oe value. Thermal treatment leads to narrowing the TMI peaks.

➢ Both in longitudinal configuration, and in transversal configuration, before and after the thermal treatment, the value of ΔZ/Z (%) ratio increases with the increase of the alternating current frequency. Thus:

- *in longitudinal configuration:*
  - for the as-deposited state, the value of ΔZ/Z (%) ratio increases rapidly when the frequency of the alternating current increases from 200 MHz to 300 MHz and, much slower, from 300 MHz to 500 MHz;
  - for the heat-treated state, the value of ΔZ/Z (%) ration increases slowly when the frequency of the current which crosses the sample increases in the 200-500 MHz range;
  - for frequencies lower than 200 MHz, both before and after the treatment, the recorded profiles are not well defined.
- *in transversal configuration*
  - increasing the frequency of the alternating current from 200 MHz to 500 MHz leads to a very small increase of the ΔZ/Z (%) ratio, for both the as-deposited samples and the heat-treated samples.

➢ According to existing data in the literature, it can be assumed that the value of ΔZ/Z (%) ratio will increase also for frequencies above 500 MHz (frequency limited by the utilised measured system) [36]. The MI effect becomes increasingly significant as the penetration depth (inversely proportional to the square root of the alternating current frequency) decreases compared to the thin film thickness investigated.

➢ Thermal treatment leads to improving of the MI response. The value of ΔZ/Z (%) ratio (for measurements performed both in longitudinal configuration, and in transversal configuration) increases by approximately 2 times (for a frequency of the alternating current of 500 MHz).

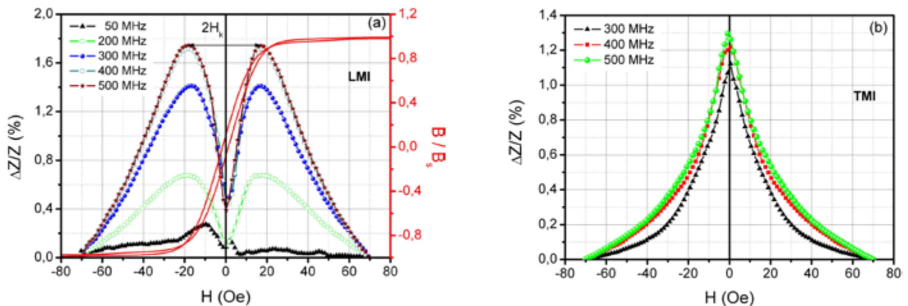

Figure 5.1: Dependence of the ΔZ/Z (%) ratio on the alternating current frequency and on the intensity of the external magnetic field (mono-layer $Fe_{73,5}Cu_1Nb_3Si_{15,5}B_7$ in as-deposited state).

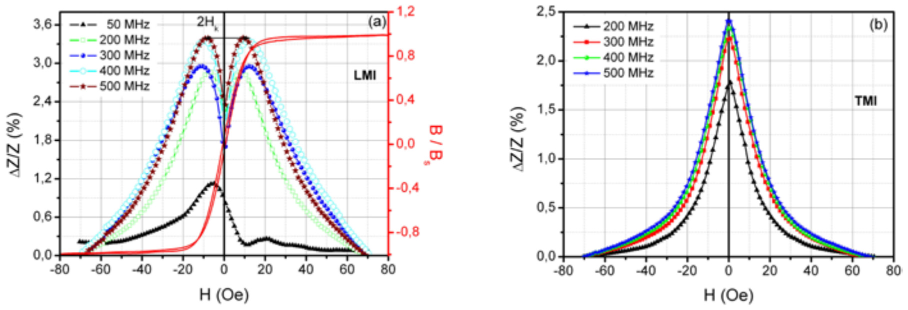

Figure 5.2: Dependence of the ΔZ/Z (%) ratio on the alternating current frequency and on the intensity of the external magnetic field (mono-layer $Fe_{73,5}Cu_1Nb_3Si_{15,5}B_7$ treated an hour at 475 °C).

5.1.2. Sandwich $Fe_{73,5}Cu_1Nb_3Si_{15,5}B_7/Cu/Fe_{73,5}Cu_1Nb_3Si_{15,5}B_7$

Figure 5.3 (a and b) and Figure 5.4 (a and b) present the dependence of the ΔZ/Z (%) ratio (LMI and TMI) on the alternating current frequency and of the intensity of the applied external magnetic field, for a sandwich $Fe_{73,5}Cu_1Nb_3Si_{15,5}B_7/Cu/$ $Fe_{73,5}Cu_1Nb_3Si_{15,5}B_7$ before (Figure 5.3 (a and b)) and after the thermal treatment (Figure 5.4 (a and b)). The thermal treatment was conducted in the thermal treatment furnace, in vacuum for 30 minutes, at the temperature of 290 °C, in the presence of a uniform external magnetic field of 500 Gauss magnetic induction, applied in the plane of the sample, in the transverse direction. The choice of a treatment temperature with a lower values than in the case of mono-layer thin films, is due to the fact that, at higher temperatures, there is the risk that the copper to diffuse into the ferromagnetic layers. The value of the applied external magnetic field didn't produce the magnetic saturation of the sample and, in these conditions, the value of ΔZ/Z (%) ratio was calculated for $Z(H_{dc})$ and $Z(H_{dc} = 0)$.

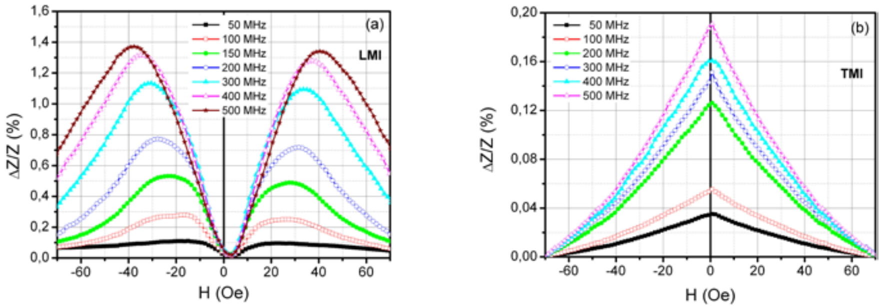

Figure 5.3: Dependence of the ΔZ/Z (%) ratio on the alternating current frequency and on the intensity of the applied external magnetic field (sandwich $Fe_{73,5}Cu_1Nb_3Si_{15,5}B_7/Cu/$ $Fe_{73,5}Cu_1Nb_3Si_{15,5}B_7$ in as-deposited state).

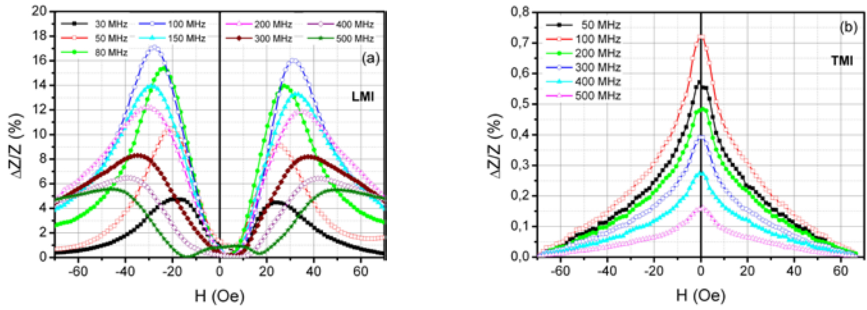

Figure 5.4: Dependence of the ΔZ/Z (%) ratio on the alternating current frequency and on the intensity of the applied external magnetic field (sandwich $Fe_{73,5}Cu_1Nb_3Si_{15,5}B_7$/Cu/ $Fe_{73,5}Cu_1Nb_3Si_{15,5}B_7$ heat-treated for 30 minutes at the temperature of 290 °C, in the presence of a magnetic field, applied in the plane of the sample, in transverse direction).

It is found that:

➢ Thermal treatment leads to decreasing the value of the magnetic field which corresponds to the maxima of the two peaks present in the LMI profiles and, respectively, narrowing the TMI peaks.

➢ For the as-deposited state (LMI and TMI), the values of ΔZ/Z (%) ratio increases with the increase of the alternating current frequency. When the value of the alternating current frequency is increased from 50 MHz to 500 MHz, the value of ΔZ/Z (%) ratio increases 14 times in longitudinal configuration and, respectively, 6 times in transversal configuration.

➢ For the heat-treated state, both in longitudinal configuration, and in transversal configuration, the value of ΔZ/Z (%) ratio increases in the frequency range 30-100 MHz, *reaching the maximum value for the frequency of 100 MHz* and decreases in the frequency range 100-500 MHz.

➢ After the thermal treatment, the value of ΔZ/Z (%) ratio, corresponding to the frequency of 100 MHz increases 60 times (LMI) and, respectively, 13 times (TMI).

General conclusions

- We obtained amorphous soft magnetic $Fe_{73,5}Cu_1Nb_3Si_{15,5}B_7$ thin films, with thicknesses from 40 nm to 1500 nm by radio frequency magnetron sputtering (RFMS) and, respectively, by high power impulse magnetron sputtering (HiPIMS). *The HiPIMS technique was utilised for the first time for the production of thin films of amorphous iron based composite materials.*
- To establish a set of optimal experimental parameters, specific to each technique, which can allow the production of amorphous thin films with superior soft

magnetic properties, and uniform surfaces, we studied their influence on the deposition rate, surface topology and the volume and surface magnetic properties of the obtained thin films. For the HiPIMS technique, the optimum set of values of the experimental parameters is: p = 10 mTorr, P_{med} = 30 W, τ = 4 μs, U = -1 kV, grounded substrate.

- In order to understand the influence of the experimental parameters values specific to HiPIMS technique on the dynamics and kinetics of plasma and the thin film growth process, we used optical, spectral and electrical technique for plasma diagnostics. The obtained results showed that with the increase of the voltage pulse, the composition of the plasma in front of the cathode undergoes major changes, leading to the initiation of the self-sputtering regime and, implicitly, to the decrease of the deposition rate of the thin films.
- The volume coercive magnetic field values of the thin films obtained by both techniques, vary according to the law $\mathbf{H_c = C/t^n}$ (t represent the thin film`s thickness, and C and n are constants whose values depend on the state of the thin films, as well as the technique and utilised conditions for their obtaining).
- For the same thickness of the thin films, the minimum value of the volume coercive magnetic field of the samples deposited by HiPIMS technique is 2 orders of magnitude lower than that of the volume coercive magnetic field corresponding to thin films deposited by RFMS technique.
- The results of the thermomagnetic analysis and the differential scanning calorimetry showed that for both techniques used, the characteristic temperatures (the Curie temperature of the ferromagnetic amorphous phase, the first crystallisation temperature and the Curie temperature of the ferromagnetic nanocrystalline phase α-Fe(Si)) of the obtained thin films are up to 70 ^{o}C lower compared to those of the ribbons utilised as targets. The characteristic temperatures values of the samples obtained by HiPIMS technique are up to 50 ^{o}C lower than those of the samples obtained by RFMS technique.
- By suitable thermal treatments applied to the amorphous material, we obtained nanocrystalline $Fe_{73,5}Cu_1Nb_3Si_{15,5}B_7$ thin films. For the thin films obtained by HiPIMS technique, as a result of thermal treatments performed at temperatures in the range 450-525 ^{o}C:
  - the volume fraction of α-Fe(Si) b.c.c. phase increases from 45,7% to 65,4%;
  - the average grain size α-Fe(Si) b.c.c. increases from 11 nm to 18 nm;
  - the silicon content of the grains α-Fe(Si) b.c.c. increases from 6,7% to 14%.
- The minimum value of the volume coercive magnetic field of thin films in nanocrystalline state is approximately 3 times (HiPIMS) and, respectively, 5 times (RFMS) smaller compared to that of the volume coercive magnetic field corresponding to amorphous state.
- We built and experimental stand for measuring the saturation magnetostriction of the thin films, utilising the cantilever method. The values are

approximately $23 \cdot 10^{-6}$ and $1 \cdot 10^{-6}$ for amorphous thin films an, respectively, nanocrystalline thin films.

- We studied the mechanical properties (modulus of elasticity, hardness, adhesion to substrate, coefficient of friction) of the thin films obtained by HiPIMS technique, by nanoindentation and nanoscratch tests. For amorphous thin films with 410 nm thickness, the values of the hardness and of the effective modulus of elasticity are approximately 9 GPa and, respectively, 146 GPa, and the average value of the coefficient of friction is approximately 0,11.
- We studied the magnetoimpedance effect for both mono-layer $Fe_{73,5}Cu_1Nb_3Si_{15,5}B_7$ thin films (600 nm), and sandwich systems $Fe_{73,5}Cu_1Nb_3Si_{15,5}B_7$/Cu/ $Fe_{73,5}Cu_1Nb_3Si_{15,5}B_7$ (600 nm/600 nm/600 nm) in the frequency range 50-500 MHz. The maximum value of $\Delta Z/Z$ (%) ratio (17.1%, LMI) was obtained for the case of sandwich type systems, thermomagnetic treated at the temperature of 290 ^{o}C, in the presence of a uniform external magnetic field (magnetic induction of 500 Gauss), applied in the plane of the sample, in transverse direction. This value is 5 times larger than the maximum values of $\Delta Z/Z$ (%) ratio recorded for mono-layer thin films, heat-treated for an hour at the temperature of 475 ^{o}C.

References:

[1] R. C. O'Handley, *Modern Magnetic Materials: Principles and Applications*, New York, Chichester: Wiley (2000);

[2] S. Tumański, Przeglad Elektrotechniczny Electrical Review **4** (2010) 1-15;

[3] K. H. J. Buschow, F. R. de Boer, *Physics of Magnetism and Magnetic Materials*, New York, Kluwer Academic Publishers (2003);

[4] S. Chikazumi, *Physics of Ferromagnetism*, Clarendon Press, Oxford (1997);

[5] B. D. Cullity, *Introduction to Magnetic Materials*, Addison-Wesley Publishing Company, Massachusetts (1972);

[6] D. Jiles, *Introduction to Magnetism and Magnetic Materials*, Chapman & Hall, New York (1995);

[7] U.S. Congress, Office of Technology Assessment, *Miniaturization Technologies*, OTA-TCT-514 (Washington, DC: U.S. Government Printing Office, November 1991);

[8] A. Zribi, J. Fortin, *Functional Thin Films and Nanostructures for Sensors. Synthesis, Physics and Applications*, Springer (2009);

[9] Oliver Gutfleisch, Matthew A. Willard, Ekkes Brück, Christina H. Chen, S. G. Sankar, J. Ping Liu, Adv. Mat. **23** (2011) 821-842;

[10] H. Gavrila and V. Ionita, J. Optoelectron. Adv. Mat. **4** (2002) 173-192;

[11] G. Herzer, *Nanocrystalline Soft Magnetic Alloys*, in Handbook of Magnetic Materials, vol. 10, edited by K.H.J. Buschow, Elsevier Science B.V., 415-462 (1997);

[12] G. Herzer, Phys. Scripta **49** (1993) 307-314;

[13] G. Herzer, M. Vazquez, M. Knobel, A. Zhukov, T. Reininger, H.A. Davies, R. Grössinger and J.L. Sanchez L., J. Magn. Magn. Mat. **294** (2005) 252-266;

[14] C. C. Koch, *Nanostructured Materials. Processing, Properties and Potential Applications*, William Andrew Publishing Norwich, New York (2002);

[15] M.E. McHenry, D.E. Laughlin, Acta Mater. **48** (2000) 223-238;
[16] M.E. McHenry, D.E. Laughlin, Prog. Mater. Sci. **44** (1999) 291-433;
[17] P. Marín, A. Hernando, J. Magn. Magn. Mat. **215-216** (2000) 729-734;
[18] A. Hernando, J.M. González, Hyperfine interact. **130** (2000) 221-240;
[19] J. M. Grenèche, J. Optoelectron. Adv. Mat. **5** (2003) 133-138;
[20] H. Gavrilă, H. Chiriac, P. Ciureanu, V. Ioniţă, A. Yelon, *Magnetism Tehnic şi Aplicat*, Editura Academiei Române, Bucureşti (2000);
[21] S. V. Vonsovski, *Magnetismul*, Editura Ştiinţifică şi Enciclopedică, Bucureşti (1981);
[22] C. Kittel, *Introduction to Solid State Physics* (4th edition), Ed. Wiley, New York (1971);
[23] F. Fiorillo, *Measurement and Characterization of Magnetic Materials*, Elsevier (2004);
[24] E. du Trémolet de Lacheisserie, D. Gignoux, M. Schlenker, *Magnetism: Materials and Applications*, Springer (2005);
[25] **I. L. Velicu**, M. Neagu, H. Chiriac, V. Tiron, M. Dobromir, IEEE T. Magn. **48** (2012) 1336-1339;
[26] **I. L.Velicu**, M. Neagu, M. Dobromir, D. Luca, N. Lupu, H. Chiriac, F. Borza, Sensor Letters **10** (2012) 902-905;
[27] **I. L. Velicu**, M. Kowalczyk, M. Neagu, V. Tiron, H. Chiriac, J. Ferenc, Mat. Sci. Eng. (B) http://dx.doi.org/10.1016/j.mseb.2013.03.002;
[28] R. W. Siegel, W. Hu, M. C. Roco, *Nanostructured Science and Technology – A Worldwide Study*, Baltimore MD: WTEC, Loyola College (1999);
[29] J. Betz, E. du Trémolet de Lacheisserie, Appl. Phys. Lett. **68** (1996) 132-133;
[30] E. du Trémolet de Lacheisserie, Phys. Rev. B **51** (1995) 15925-15932;
[31] E. du Trémolet de Lacheisserie, J.C. Peuzin, J. Magn. Magn. Mater. **136** (1994) 189-196;
[32] E. van de Riet, J. Appl. Phys. **76** (1994) 584-586;
[33] N.H. Duc, *Giant mangnetostriction in lanthanide-transition metal thin films*, in Handbook on the physics and chemistry of rare earths, vol. 32, ed. K. A. Gschneidner, Jr., L. Eyring, and G. H. Lander (North-Holland, Amsterdam), 2001;
[34] E. Klokholm, IEEE T. Magn. **12** (1976) 819-821;
[35] C. Tannous, J. Gieraltowski, J. Mater. Sci-Mater. El. **15** (2004) 125-133;
[36] M. H. Phan, Hua-Xin Peng, Prog. Mater. Sci. 53 (2008) 323-420;
[37] D.C. Jiles, Acta Mater. **51** (2003) 5907-5939;
[38] J.Q. Yu, Y. Zhou, B.C. Cai, aX.L. Zhao, Acta Metall. Sinic. **13** (2000) 995-1000;
[39] M. A. Corrêa, A. D. C. Viegas, R. B. da Silva, A. M. H. de Andrade, R. L. Sommer, J.Appl. Phys. **101** (2007) 043905;
[40] T. Uchiyama, K. Mohri, L. Panina, K. Furuno, IEEE T. Magn. **31** (1995) 3182-3184;
[41] J. Moulin, M. Woytasik, I. Shahosseini, Microsyst. Technol. **17** (2011) 637-644;
[42] L. V. Panina, K. Mohn, T. Uchyama, M. Noda, IEEE T. Magn. **31** (1995) 1249-1260;
[43] S. Xiao, Y. Liu, S. Yan, Y. Dai, L. Zhang, L. Mei, Phys. Rev. (B) 61 (2000) 5734-5739;
[44] L. V. Panina, K. Mohri, Appl. Phys. Lett. **65** (1994) 1189-1191;
[45] L. Brunetti, M. Coisson, P. Tiberto, F. Vinai, H. Chiriac, F. Borza, Sensor. Actuat. A-Phys. **91** (2001) 203-206;
[46] B. Bhushan, *Handbook of Nanotechnology*, Springer (2010);
[47] A. C. Fischer-Cripps, *The IBIS Handbook of Nanoindentation*, Fischer-Cripps Laboratories (2005);
[48] A. C. Fischer-Cripps, *Introduction to Contact Mechanics*, Springer (2007);
[49] B. Bhushan, L. Xiaodong, Int. Mater. Rev. **48** (2003) 125-164;
[50] W.C. Oliver, G. M. Pharr, J. Mater. Res. **19** (2004) 3-20;
[51] C. Shaohua, L. Lei, W. Tzuchiang, Acta Mech. Sinica **20** (2004) 383-392;
[52] R. Saha, W.D. Nix, Acta Mater. **50** (2002) 23-38;

[53] K. Seshan, *Handbook of Thin-Film Deposition Processes and Techniques Principles, Methods, Equipment and Applications* (2th edition), William Andrew Publishing (2002);
[54] B.N. Chapman: *Glow discharge processes*, New York: Wiley (1980);
[55] M. A. Lieberman, A. J. Lichtenberg, *Principles of Plasma Discharges and Materials Processing* (2th edition), John Wiley & Sons (2005);
[56] A. Bogaerts, E. Neyts, R. Gijbels, J. van der Mullen, Spectrochim. Acta Part B **57** (2002) 609-658;
[57] G. Popa, L. Sârghi, *Bazele fizicii plasmei*, Ed. Univ. Al. I. Cuza, Iaşi (2000);
[58] P. J. Kelly, R. D. Arnell, Vacuum, **56** (2000) 159-172;
[59] K.H. Maria, S.P. Mondal, S. Choudhury, S.S. Sikder, M.A. Hakim, D.K. Saha, J. Emerg. Trends. Eng. Appl. Sci. **2** (2011) 102-108;
[60] R.M. Bozoroth, *Ferromagnetism*, p. 74, D. Van Nostrand Company, Inc., Princeton, NJ (1964);
[61] M. Neagu, *Elipsomterie. Magneto-optică*, Editura şi tipografia Stef, Iaşi (2007);
[62] C.S. Grommé, T.L. Wright, D.L. Peck, J. Geophys. Res. **74** (1969) 5277-5293;
[63] Tauxe, L., *Paleomagnetic Principles and Practice*, 1st ed., p. 299, Springer, New York, 1998;
[64] A. Neuweiler, H. Kronmüller, J. Magn. Magn. Mat. **177** (1998) 1269-1270.

Dissemination of scientific activity during doctoral studies

I. Papers published or submitted for publication in ISI journals

1. M. Dobromir, M. Neagu, H. Chiriac, C. Agheorghiesei, A. Bulai, **L. Velicu**, *Ellipsometric investigation of Fe-based amorphous thin films*, Optoelectronics and Advanced Materials - Rapid Communications **4** (2010) 1667-1669 (factor de impact – 0,477; AIS – **0,077**);
2. **I. L. Velicu**, M. Neagu, M. Dobromir, D. Luca, N. Lupu, H. Chiriac, F. Borza, *Structural, Magnetic and Magnetoelastic Behaviour of FeCuNbSiB Thin Films*, Sensors Letters **10** (2012) 902-905 (factor de impact – 0,517; AIS – **0,117**);
3. **I. L. Velicu**, M. Neagu, H. Chiriac, V. Tiron, M. Dobromir, *Structural and Magnetic Properties of FeCuNbSiB Thin Films Deposited by HiPIMS*, IEEE Transactions on Magnetics, **48** (2012) 1336-1339 (factor de impact – 1,422; AIS – **0,419**);
4. **I. L. Velicu**, M. Kowalczyk, M. Neagu, V. Tiron, H. Chiriac, J. Ferenc, *FINEMET-type thin films deposited by HiPIMS: influence of growth and annealing conditions on the magnetic behaviour*, Materials Science & Engineering B (2013), http://dx.doi.org/10.1016/j.mseb.2013.03.002, (factor impact – 1,846; AIS – **0,535**);
5. **I. L. Velicu**, M. Neagu, L. Costinescu, D. Munteanu, E. P. Koumoulos, C. A. Charitidis, *Nanomechanical Properties of amorphous FeCuNbSiB Thin Films Deposited by HiPIMS*, Sensors Letters, acceptată pentru publicare (factor de impact – 0,517; AIS – **0,117**);
6. **I. L. Velicu**, V. Tiron, G. Popa, *Dynamics of the fast - HiPIMS discharge during FINEMET - type films deposition*, Surface and Coatings Technology, trimisă spre publicare (factor de impact – 1,941; AIS – **0,57**);
7. V. Tiron, **I L.Velicu**, F. Ghiorghiu, G. Popa, *The effect of the additional magnetic field and gas pressure on the sheath region of a high power impulse magnetron sputtering discharge*, Romanian Reports in Physics, trimisă spre publicare (factor de impact – 1,123; AIS – **0,125**).

II. Papers accepted for publication in the proceeding of international conferences

1. V. Tiron, C. Vitelaru, **I-L.Velicu**, F. Ghiorghiu, G. Popa, *On transport phenomena in high power pulse unbalanced magnetron discharge with additional external magnetic field*, Proceeding of the XXXI International Conference on Phenomena in Ionized Gases – ICPIG;
2. M. Dobromir, **L. I. Velicu**, M. Neagu, H. Chiriac, *FeCuNbSiB Thin Films Deposited by Pulsed Laser Deposition: Structural and Magnetic Propertie*s, Proceeding of the International Conference Nanomaterials: Application & Properties – NAP.

III. Papers presented at national conferences

1. **I.L. Velicu**, M. Dobromir, M. Neagu, H. Chiriac, D. Luca, N. Lupu, V. Pohoaţă, B. Munteanu, *FeCuNbSiB Thin Films Deposited by RF Magnetron Sputtering*, the XL Naţional Conference Physics and Modern Educational Technologies, 12-14 May 2010, Iaşi, Romania (**oral**);
2. **I. L. Velicu**, M. Neagu, *FeCuNbSiB thin films deposited by HiPIMS: influence of deposition conditions and thermal treatment*, Doctoral School Conference, 21-22 October 2011, Iaşi, Romania (**oral**);
3. **I.L. Velicu**, V. Tiron, G. Popa, *Onset of sustained self-sputtering regime in HiPIMS discharge for growing FINEMET-type thin films*, Doctoral School Conference, 19 October 2012, Iaşi, Romania (**oral**);
4. **I.L. Velicu**, V. Tiron, G. Popa, *FINEMET-type thin films obtained by HiPIMS: influence of deposition conditions on the deposition rate*, The 5th National Conference of Applied Physics – CNFA 2013, 23-24 May 2013, Iaşi, Romania (**poster**).

IV. Papers presented at international conferences

1. **I.L. Velicu**, M. Neagu, N. Lupu, H. Chiriac, V. Tiron, M. Dobromir, *FeCuNbSib Thin Films Deposited by HiPIMS: Annealing Influence on the Structural and Magnetic Properties*, The 5th International Workshop on Amorphous and Nanostructured Magnetic Materials – ANMM 2011, 5-7 September 2011, Iaşi, Romania (**poster**);
2. **I.L. Velicu**, M. Neagu, H. Chiriac, V. Tiron M. Dobromir, *Structural and Magnetic Properties of FeCuNbSiB Thin Films Deposited by HiPIMS*, The 20th Soft Magnetic Materials Conference – SMM20, 18-22 September 2011, Kos Isle, Greece (**poster**);
3. **I. L. Velicu**, M. Neagu, H. Chiriac, V. Tiron, M. Dobromir, V. Pohoaţă, B. Munteanu, *Effect of preparation conditions on magnetic properties of FeCuNbSiB thin films*, The 10th International Conference on Global Research And Education – inter-Academia 2011, 26-29 September 2011, Suceviţa, Romania (**oral/poster**);
4. M. Dobromir, **L.I. Velicu**, M. Neagu, H. Chiriac, *Structural and magnetic properties of pulsed laser deposited FeCuNbSiB thin films*, International Conference on Materials and Applications for Sensors and Transducers – IC-MAST 2012, 24-28 May 2012, Budapest, Hungary (**poster**);

5. E.P. Koumoulos, **I.L. Velicu**, V.P. Tsikourkitoudi, C.A. Charitidis, M. Neagu, V. Tiron, *Nanomechanical properties of FINEMET-type thin films deposited by HiPIMS for sensing applications*, The 9th International Conference on Nanosciences & Nanotechnologies (NN12), 3-6 July 2012, Thessaloniki, Greece (**poster**);
6. **I.L. Velicu**, M. Kowalczyk, M. Neagu, V. Tiron, H. Chiriac, J. Ferenc, *FINEMET-type thin films deposited by HiPIMS: influence of growth and annealing conditions on the magnetic behaviour*, The 9th International Conference on Physics of Advanced Materials – ICPAM-9, 20-23 September 2012, Iaşi, Romania (**poster**);
7. V. Tiron, **I.L. Velicu**, C. Costin, G. Popa, *Dynamics of the fast - HiPIMS discharge during FINEMET-type films deposition*, The 4th International Conference on Fundamentals and Industrial Applications of HIPIMS, 12-13 June 2013, Braunschweig, Germany (**oral**);
8. V. Tiron, **I L.Velicu**, F. Ghiorghiu, G. Popa, *The effect of the additional magnetic field and gas pressure on the sheath region of a high power impulse magnetron sputtering discharge*, The 16th International Conference on Plasma Physics and Applications – CPPA 2013, 20-25 June 2013, Bucharest, Romania (**poster**);
9. V. Tiron, C. Vitelaru, **I-L.Velicu**, F. Ghiorghiu, G. Popa, *On transport phenomena in high power pulse unbalanced magnetron discharge with additional external magnetic field*, XXXI International Conference on Phenomena in Ionized Gases – ICPIG 2013, 14-19 July 2013, Granada, Spain (**poster**);
10. M. Dobromir, **L. I. Velicu**, M. Neagu, H. Chiriac, *FeCuNbSiB Thin Films Deposited by Pulsed Laser Deposition: Structural and Magnetic Properties*, Nanomaterials: Application & Properties – NAP 2013, 16-21 September 2013, Alushta, Ukraine (**poster**).

V. Awards

1. **Premiul II** – **I.L. Velicu**, M. Dobromir, M. Neagu, H. Chiriac, D. Luca, N. Lupu, V. Pohoaţă, B. Munteanu, *FeCuNbSiB Thin Films Deposited by RF Magnetron Sputtering*, a XL-a Conferinţa Naţională Fizica şi Tehnologiile Educaţionale Moderne, 12-14 mai 2010, Iaşi, România (**oral**);
2. **Premiul oferit de Royal Society of Chemistry (U.K.) pentru cel mai bun poster** şi **Honorable Mention oferită de comitetul de organizare** – M. Dobromir, **L. I. Velicu**, M. Neagu, H. Chiriac, *FeCuNbSiB Thin Films Deposited by Pulsed Laser Deposition: Structural and Magnetic Properties*, Nanomaterials: Application & Properties – NAP 2013, 16-21 septembrie 2013, Alushta, Ucraina (**poster**).

VI. Other activities

1. **Scientific reviewer** – IEEE Transactions on Magnetics, 2011.